Published in final edited form as:
Mol Imaging Biol. 2012 June ; 14(3): 336–347. doi:10.1007/s11307-011-0500-8.

An Engineered Cysteine-Modified Diabody For Imaging Activated Leukocyte Cell Adhesion Molecule (ALCAM)-Positive Tumors

Katelyn E. McCabe[1], **Bin Liu**[2], **James D. Marks**[2,3], **James S. Tomlinson**[4], **Hong Wu**[5], and **Anna M. Wu**[1]

[1]Crump Institute for Molecular Imaging, Department of Molecular and Medical Pharmacology, David Geffen School of Medicine at University of California, Los Angeles, Los Angeles, California

[2]Department of Anesthesia, University of California, San Francisco, San Francisco, California

[3]Department of Pharmaceutical Chemistry, University of California, San Francisco, San Francisco, California

[4]Division of Surgical Oncology, David Geffen School of Medicine at University of California, Los Angeles, Los Angeles, California

[5]Department of Molecular and Medical Pharmacology, David Geffen School of Medicine at University of California, Los Angeles, Los Angeles, California

Abstract

Purpose—To generate and evaluate a positron emission tomography (PET) radiotracer targeting activated leukocyte cell adhesion molecule (ALCAM/CD166).

Procedures—A human anti-ALCAM single chain variable fragment was reformatted to produce a covalent dimer, termed a cys-diabody (CysDb). Purified CysDb was characterized by gel electrophoresis and size exclusion chromatography, and immunoreactivity was assessed by flow cytometry and immunofluorescence. Targeting and imaging of ALCAM-positive tumors using ^{64}Cu-DOTA-CysDb were evaluated in mice bearing human pancreatic adenocarcinoma xenografts (HPAF-II or BxPC-3).

Results—CysDb binds specifically to ALCAM-positive cells *in vitro* with an apparent affinity in the range of 1–3 nM. MicroPET images at 4 h showed specific targeting of positive tumors *in vivo*, a finding confirmed by biodistribution analysis, with positive-to-negative tumor ratios of 1.9±0.6 and 2.4±0.6, and positive tumor-to-blood ratios of 2.5±0.9 and 2.9±0.6 (HPAF-II and BxPC-3, respectively).

Conclusions—Successful imaging with ^{64}Cu-DOTA-CysDb in animal models suggests further investigation of ALCAM as an imaging biomarker is warranted.

Keywords

activated leukocyte cell adhesion molecule (ALCAM); biomarker; diabody; pancreatic cancer; positron emission tomography (PET)

Corresponding author: Anna M. Wu, awu@mednet.ucla.edu, Phone: 310-794-5088, Fax: 310-206-8975.

Conflict of Interest

Anna M. Wu owns stock and is a consultant to ImaginAb, Inc. The other authors declare they have no conflicts of interest.

Introduction

Scientific and technological advancements in the past two decades have allowed the identification of cancer biomarkers that can provide important information during various stages of disease management. Measurement of a biomarker that is expressed at an abnormal level during disease progression can be useful for initial detection of cancer and shed light on prognosis. The status of a predictive tumor marker can be helpful in determining whether the individual is a candidate for a particular targeted therapeutic. Furthermore, a change in biomarker expression can be an indicator of response to therapy or recurrence of disease. The identification of tumor tissue biomarkers has, in turn, led to the production, validation, and FDA-approval of a number of antibody-based targeted therapeutics that play a role in disease management. As a result of the potential utility of complementary imaging agents for this class of immunotherapeutics, antibody-based positron emission tomography (PET), or immunoPET, has generated considerable interest. This imaging modality takes advatange of the high sensitivity, resolution, and quantitation offered by PET, as well as the intrinsic specificity of antibodies [1].

To generate PET images that show delineation of antigen-positive tumors, sufficient radiotracer uptake by the target tissue and blood clearance are both necessary. These pharmacokinetic properties, a function of the antibody in the case of an immunoPET agent, determine the tracer uptake time required to achieve high contrast. Due to the interaction of the Fc portion of an intact antibody and neonatal Fc receptors, a full-length IgG can undergo recycling and persist in the circulation for 1–3 weeks, making this targeting molecule format unsuitable for same- or next-day imaging applications [2]. Engineered antibody fragments that lack the Fc region, such as single-chain variable fragments (scFv) and non-covalent scFv dimers (diabodies; Db), have serum half-lives in the range of 0.5–7 h, which are compatible with rapid imaging [2]. Diabodies exhibit higher tumor uptake than scFvs due to their greater avidity, making them superior targeting molecules for imaging, with maximum tumor-to-blood ratios reached at 2–6 h post-injection [3] and high-contrast images generated as early as 1 h post-injection [4]. Addition of cysteine residues at the C-termini of diabodies results in the production of covalent cysteine-modified diabodies (CysDb) that possess a reactive group located away from the antigen-binding site to which cargo can be conjugated using thiol-specific chemistry [5,6]. This engineered modification allows for site-specific radiolabeling, which can help preserve the immunoreactivity of the radionuclide-conjugated molecule.

Activated leukocyte cell adhesion molecule (ALCAM/CD166) has recently been shown to be clinically relevant in many cancers, including breast [7–9], colorectal [10], oral [11], ovarian [12], pancreatic [13], and prostate [14,15], making it worthy of further investigation. For malignancies such as pancreatic adenocarcinoma, which are diagnosed late and lack effective systemic treatments, an informative imaging agent could have a significant clinical impact by aiding in staging and treatment decisions. Named for its initial identification as a CD6 ligand expressed on activated leukocytes [16,17], ALCAM is a 100 kDa cell surface glycoprotein that also participates in homotypic interactions [17]. While the role of ALCAM in tumorigenesis is still not well understood, *in vitro* and *in vivo* animal studies using a melanoma model suggest that ALCAM-ALCAM interactions promote primary tumor growth [18]. Not surprisingly, the presence or absence of these homotypic interactions, as well as the engagement of ALCAM's ligand-binding domains, also appears to influence the metastatic potential of a tumor. In further animal studies using a melanoma model, increased metastasis was observed with overexpression of a truncated version of ALCAM that lacks the ligand-binding module, while decreased metastatic capacity was seen with expression of a soluble version of ALCAM that binds this module [18,19]. In addition to its clinical

relevance, ALCAM's upregulation on the surface of cancer cells relative to normal cells [10,13,14] makes this molecule a good candidate target for molecular imaging.

Previously, an internalizing anti-ALCAM scFv hat demonstrated binding to prostate cancer cells was isolated from a naïve human scFv library [20,21]. To assess the potential of ALCAM as a therapeutic target, this anti-ALCAM scFv was conjugated to liposomes loaded with various chemotherapeutics [22]. In the present work, the anti-ALCAM scFv was reformatted to produce a CysDb in order to examine the potential of ALCAM as an imaging target. *In vivo* targeting and microPET imaging with ^{64}Cu-DOTA-CysDb was evaluated using ALCAM-positive human pancreatic adenocarcinoma xenografts in nude mice as a model system.

Materials and Methods

Cell lines and media

The human pancreatic adenocarcinoma cell lines BxPC-3 (ATCC #CRL-1687) and HPAF-II (ATCC #CRL-1997) were maintained in RPMI 1640 (Mediatech, Inc.) supplemented with 10% fetal bovine serum (FBS). The rat glioma cell line C6 (ATCC #CCL-107) was maintained in Deficient Dulbecco's Modification of Earl's Basal Media (DME) High Glucose (IrvineScientific) supplemented with 10% FBS and 1% L-glutamine. NS0 mouse myeloma cells (Sigma) [23] were maintained as described [24].

Evaluation of ALCAM expression on cell lines

ALCAM expression of cell lines was evaluated by flow cytometry. Cells were harvested and resuspended in PBS/1% FBS to a concentration of 10^6 cells/mL. Approximately 2×10^5 cells were incubated with 4 μg mouse anti-human CD166 monoclonal antibody (AbD Serotec) for 1 hour on ice, washed with PBS/1% FBS, and centrifuged at 1200*g*. Cells were resuspended in 200 μL PBS/1% FBS and incubated with 4 μg R-Phycoerythrin (PE)-conjugated goat $F(ab')_2$ anti-mouse IgG, Fcγ-specific antibody (Jackson ImmunoResearch Laboratories, Inc.) for 45 minutes on ice. Cells were washed and centrifuged, and resuspended in 0.5 mL PBS. For quantitative flow cytometry, samples were prepared in duplicate or triplicate using the QIFI kit (Dako) and specific antibody-binding capacity (SABC) was calculated according to the manufacturer's instructions. Data were acquired using a FACScan flow cytometer (BD Biosciences) and analysis was performed using CellQuest software (BD Biosciences).

Design and construction of anti-ALCAM CysDb

Overlap-extension PCR was used to amplify the V_H and V_L genes from the anti-ALCAM scFv H3 [20]. The C-terminal cysteine residue, hexahistidine tag, and *Eco*RI restriction site of H3 were retained, an *Xba*I restriction site and mammalian leader sequence containing a secretion signal were introduced at the N-terminus, and the GlySer-rich linker was reduced from 15 to 8 amino acids to induce diabody formation [5]. The anti-ALCAM CysDb construct was cloned into the mammalian expression vector pEE12 [25] and confirmed by DNA sequencing.

Expression and Screening

Approximately 2×10^6 NS0 cells were transfected with 13 μg *Sal*I-linearized DNA using a Multiporator (Eppendorf) and grown in selective glutamine-deficient Dulbecco's Modification of Eagle's Medium (DMEM) (Mediatech, Inc.) as previously described [25]. Supernatants from individual clones were assayed for CysDb production by SDS-PAGE followed by western blotting; nitrocellulose membranes (Bio-Rad) were probed with 0.2 μg/

mL alkaline phosphatase (AP)-conjugated Protein A (Sigma) and developed with the NBT/BCIP Color Development Substrate Kit (Promega).

Production and purification

The highest anti-ALCAM CysDb-producing clone based on westerns was selected for terminal culture in triple flasks (Corning) containing 350 mL selective media. Supernatant was filtered through a 0.22 μm polyethersulfone (PES) membrane (Corning) and directly loaded onto a 1.6 mL Protein A (Thermo Fisher Scientific Inc.) column at a flow rate of 1 mL/min using an AKTA purifier (GE Healthcare Life Sciences). The loaded column was equilibrated with PBS, and anti-ALCAM CysDb was eluted using a 0–20% gradient of 0.1 M citric acid, pH 2.0. 1 mL elution fractions were collected into tubes containing 0.5 mL 1.0 M Tris buffer, pH 8.2. Pre-cast 4–20% Tris-HCl SDS-PAGE gels (Bio-Rad) were loaded with aliquots of fractions and an anti-HER2 CysDb of known molecular weight derived from the sequence of trastuzumab [6,26], electrophoresed, and stained with InstantBlue (Novexin/Expedeon). Fractions containing purified anti-ALCAM CysDb were pooled and dialyzed against PBS using a Slide-A-Lyzer Dialysis Cassette (10,000 Da MWCO; Pierce Biotechnology). Protein concentration was determined by A_{280} using a predicted extinction coefficient of 1.6 mg/mL based on the amino acid composition.

Biochemical characterization of anti-ALCAM CysDb

Anti-ALCAM CysDb and the aforementioned anti-HER2 CysDb were reduced using 75 mM dithiothreitol (DTT) and analyzed by SDS-PAGE as described above. Anti-ALCAM CysDb was further analyzed by size exclusion chromatography using a 24 mL Superdex 75 column (GE Healthcare Life Sciences) on an AKTA Purifier. CysDb was loaded onto the column with PBS at a flow rate of 0.5 mL/min and A_{280} was monitored during elution.

Functional characterization of anti-ALCAM CysDb

Flow cytometry—Cells were prepared as described above. Three rounds of incubations were carried out on ice. The first was with 4 μg anti-ALCAM CysDb for 1 hour, the second with 0.2 μg mouse anti-Penta-His antibody (QIAGEN) for 45 minutes, and the third with 4 μg PE-conjugated goat anti-mouse antibody for 30 minutes. Cells were washed, centrifuged, and resuspended in between incubations as described above. To estimate affinity, cells were incubated with various concentrations of anti-ALCAM CysDb, ranging from 0.01 nM to 31.6 nM, followed by the amounts of detection antibodies listed above.

Immunofluorescence—Approximately 0.75 mg anti-ALCAM CysDb in 0.5 mL PBS was labeled with Alexa Fluor 647 using a protein labeling kit according to the manufacturer's instructions (Molecular Probes). Purification of the labeled protein was carried out using dye removal columns (Thermo Fisher Scientific Inc.). Degree of labeling was calculated from A_{280} and A_{647}, using the A_{280} correction factor (0.03) and extinction coefficient (239,000 $cm^{-1}M^{-1}$) of Alexa Fluor 647, and the predicted extinction coefficient (83,240 $cm^{-1}M^{-1}$) of anti-ALCAM CysDb. For immunofluorescence experiments, cells were grown to approximately 50% confluency on a Lab-TekII Chamber Slide (Thermo Fisher Scientific Inc.) and incubated with 0.5 mL media and 4 μg Alexa Fluor 647-CysDb conjugate for 1 h at 4°C. Cells were then washed with PBS/1% FBS, fixed with 3.7% formaldehyde, and stained with 4′,6-diamidino-2-phenylindole (DAPI). Slides were viewed at 20x magnification using an Axio Imager D1 microscope (Zeiss) and digital image processing was performed using AxioVision software (Zeiss).

Radiolabeling of anti-ALCAM CysDb

Anti-ALCAM CysDb was dialyzed against Chelex 100-treated (1.2 g/L; Bio-Rad) 50 mM sodium borate buffer, pH 8.5, and concentrated to 1.2–1.4 mg/mL using a 10 kDa MWCO Vivaspin 20 spin column (Sartorius Stedim Biotech). 1.2–1.4 mg anti-ALCAM CysDb was incubated with 1,4,7,10-tetraazacyclododecane-1,4,7,10-tetraacetic acid mono (DOTA-NHS-ester) (Macrocyclics) for 12–16 h at 4°C. The DOTA-NHS-ester to CysDb molar ratio in this conjugation reaction was approximately 200:1. After conjugation, the reaction solution was applied to a PD-10 column (Amersham Biosciences) equilibrated with Chelex-treated PBS. 300 μL elution fractions were collected, and those with high A_{280} readings were pooled. Conjugation efficiency was assessed qualitatively by size exclusion chromatography using a Superdex 75 column on an AKTA purifier. 40–50 μL 0.1 M Chelex-treated ammonium citrate, pH 5.5, and 0.4–0.5 mCi of ^{64}Cu (MDS Nordion or Washington University), diluted to ~0.1 mCi/μL with 0.25 M Chelex-treated ammonium acetate, pH 7.0, were added to 200–300 μg DOTA-conjugated CysDb in 200–250μL Chelex-treated PBS, for a total reaction volume between 250–300 μL. The reaction was incubated at 43°C for 50 min. Labeling efficiency was determined using monoclonal antibody instant thin layer chromatography (ITLC) strips (Biodex medical systems). Briefly, 2 μL reaction was spotted at the origin of the strip and the strip was immediately placed in a vial containing 1 mL saline. The strip was removed from the saline when the solvent reached the front line, and cut at the cut line, separating sections 1 and 2. Activities of the sections were counted using a Wizard 3″ 1480 Automatic Gamma Counter (Perkin-Elmer), and labeling efficiency was calculated by dividing protein-bound activity (section 1) by total activity (sum of sections 1 and 2).

MicroPET imaging

Tumor implantation—All animal studies were performed under an approved UCLA Chancellor's Animal Research Committee protocol. Cells for implantation were prepared on ice. 1–3.3 × 10^6 cells were resuspended in DMEM, mixed with an equal volume of Matrigel (BD Biosciences), and injected subcutaneously in the shoulder regions of female nude mice (Charles River Laboratories International, Inc.) 9–24 days prior to microPET imaging. In 5 mice, HPAF-II and C6 cells were injected in the left and right shoulder regions, respectively. In 4 mice, BxPC-3 and C6 cells were injected in the left and right shoulder regions, respectively. Tumors were not implanted in the female *Alcam*$^{-/-}$ mice (courtesy of Dr. George Weiner, University of Iowa).

Imaging—200 μL doses were prepared by added saline and human serum albumin (HSA; 4% final concentration) to 100–165 μCi ^{64}Cu-DOTA-CysDb, and injected into the tail vein of each mouse. At 4 and 21 h post-injection, mice were anesthetized using 2% isoflurane, and 10-minute static scans were taken using a Focus microPET scanner (Concorde Microsystems). Filtered back-projection (FBP) was used for image reconstruction. Two or three mice in each group were also imaged in a microCT scanner (ImTek) immediately following microPET imaging.

Biodistribution

At 21 h post-injection, tumor-bearing mice were sacrificed, tumors and organs were collected and weighed, and activity was counted using the gamma counter mentioned above. Activity values were decay-corrected to the time of injection, and percent injected dose per gram (%ID/g) was calculated for each tumor and organ. At 4 h post-injection, non-tumor-bearing *Alcam*$^{-/-}$ mice were sacrificed and analyzed similarly. T-tests were performed to determine statistical significance.

Region of interest analysis

Region of interest (ROI) analysis of images acquired at 4 and 21 h was performed using AMIDE [27]. Images were normalized to activity of the injected dose and animal body weight, and scaled using the same maximum and minimum standard uptake values (SUV). Images were displayed as coronal slices 2 mm thick, and ellipsoidal ROIs of similar size covering the area of the ALCAM-positive tumor were drawn on each coronal slice in which the tumor was distinguishable. When available, a co-registered CT scan was used as an anatomical guide. ROI statistics were generated, and the product of the mean (image units/volume/time), volume, and time was calculated to determine the total image units in each ROI. Total image units were converted into total activity using a conversion factor determined from ROI analysis of a copper-64 phantom, and activity was decay-corrected back to the time of dose calibration and injection for calculation of the %ID/g for each ROI. The average of these values was then calculated to determine the tumor %ID/g for comparison with the uptake value calculated from the *ex vivo* biodistribution analysis. For each image, 5 ROIs were also drawn on neck muscle. Average image units in these ROIs was calculated and compared to average image units for the corresponding positive tumor to determine tumor-to-background signal ratios.

Immunohistochemistry

In a separate set of mice, tumors were harvested 3 wk after implantation of cells, fixed in 4% formaldehyde overnight, and paraffin-embedded. 4 μm sections were cut, and samples were deparaffinized, rehydrated, and subjected to heat-induced epitope retrieval (HIER). Slides were incubated with a 1:50 dilution of anti-CD166 mouse monoclonal antibody (Vector) for 2 h at room temperature, and signal was detected using the mouse EnVision+ System-HRP (DAB) kit (Dako). Sections were counterstained with hematoxylin. Slides were converted to digital images at 20x magnification using a ScanScope XT digital slide scanner (Aperio) and viewed using ImageScope Viewer (Aperio).

Results

Identification of ALCAM-positive and –negative cell lines

Qualitative flow cytometry analysis using a mouse monoclonal anti-human CD166 antibody showed that the human pancreatic adenocarcinoma cell lines HPAF-II and BxPC-3 are both positive for cell surface ALCAM, while the rat glioma cell line C6 is negative (see Fig. 1a). Quantitative analysis using calibrated beads and the same monoclonal antibody confirmed that cell surface expression on the two positive cell lines is high, with HPAF-II and BxPC-3 cells both having specific antibody-binding capacity (SABC) values between 250,000 and 300,000 ($n = 2$; not shown).

Production and biochemical characterization of anti-ALCAM CysDb

The linker between the V_H and V_L genes of the anti-ALCAM scFv was shortened from 15 to 8 amino acids, and an N-terminal *Xba*I restriction site and mammalian leader sequence were introduced to produce the CysDb construct (see Fig. 1b). Schematic representations of the unreduced and reduced forms of anti-ALCAM CysDb are shown in Figure 1c. Anti-ALCAM CysDb was purified from NS0 terminal cultures with a yield of ~10 mg/L supernatant. SDS-PAGE analysis showed that anti-ALCAM CysDb migration under non-reducing conditions is consistent with its predicted dimeric molecular weight of approximately 50 kDa, and under reducing conditions is consistent with its predicted monomeric molecular weight (see Fig. 2a). Size exclusion chromatography confirmed production of an scFv dimer, as the anti-ALCAM CysDb elution time (23.8 min) is similar

to that of the anti-HER2 CysDb (22.5 min) (see Fig. 2b, [6]). The lack of additional bands on the SDS-PAGE gel and the single peak on the chromatogram indicate high purity.

Functional characterization of anti-ALCAM CysDb

Flow cytometry data showed specific binding of anti-ALCAM CysDb to the ALCAM-positive cell lines (HPAF-II and BxPC-3), with minimal nonspecific binding of the secondary and tertiary detection antibodies (see Fig. 3a). Alexa Fluor 647 was successfully conjugated to anti-ALCAM CysDb, and A_{280} and A_{647} of the conjugate indicated an average of 1–2 moles Alexa Fluor 647 per mole anti-ALCAM CysDb. The fluorescent microscopy images in Figure 3b show that Alexa Fluor 647-anti-ALCAM CysDb retains immunoreactivity and binds specifically to ALCAM-positive cells. To evaluate the affinity of anti-ALCAM CysDb, flow cytometry was performed to obtain the equilibrium binding constant (K_D). The affinity was determined to be in the range of 1–3 nM (see Fig. 3c).

DOTA-conjugation and radiolabeling of anti-ALCAM CysDb

Anti-ALCAM CysDb was conjugated to a bifunctional DOTA-NHS-ester chelator and subsequently radiolabeled with ^{64}Cu to produce an imaging agent for use with PET. Size exclusion chromatography showed that DOTA-conjugated anti-ALCAM CysDb eluted slightly earlier (22.4 min) than unconjugated anti-ALCAM CysDb, and the large peak area corresponding to the conjugate indicates high conjugation efficiency (data not shown). ^{64}Cu labeling efficiency of DOTA-anti-ALCAM CysDb was 82±11% (n = 4).

MicroPET imaging using ^{64}Cu-DOTA-anti-ALCAM CysDb

To test the utility of ^{64}Cu-DOTA-anti-ALCAM CysDb as a microPET imaging agent, doses containing 60–90 μg protein and 100–165μCi (85–95 Ci/mmol) were injected into the tail veins of mice bearing an ALCAM-positive (HPAF-II or BxPC-3) subcutaneous tumor in the left shoulder area, and an ALCAM-negative (C6) subcutaneous tumor in the right shoulder area. MicroPET images showing demarcation of ALCAM-positive tumors were obtained at 4 h post-injection of ^{64}Cu-DOTA-anti-ALCAM CysDb (see Fig. 4a). ALCAM-negative tumors were not clearly visible. Very high signal in the kidneys and liver is also evident. *Ex vivo* gamma counting of tumors and organs harvested at 21 h post-injection confirmed specific targeting of the probe, with positive tumor uptakes of 1.8 ± 0.5 %ID/g and 2.5 ± 0.5 %ID/g (HPAF-II and BxPC-3, respectively; p =.08), and negative tumor uptakes of 1.0 ± 0.1 %ID/g, a level comparable to that seen in the blood (0.7± 0.1 % ID/g for HPAF-II tumor-bearing mice, $p < .01$; 0.9 ± 0.1 %ID/g for BxPC-3 tumor-bearing mice, $p > .1$). Differences in uptake between ALCAM-positive and ALCAM-negative tumors were statistically significant ($p < 0.01$ for both HPAF-II vs. C6 and BxPC-3 vs. C6). Tumor uptake values result in positive tumor-to-negative tumor ratios of 1.9 ± 0.6 and 2.4± 0.6 (HPAF-II:C6 and BxPC-3:C6, respectively), and positive tumor-to-blood ratios of 2.5±0.9 and 2.9 ±0.6 (HPAF-II:blood and BxPC-3:blood, respectively). Liver and kidney uptake values were high for both tumor-bearing mice and *Alcam*$^{-/-}$ mice. Uptake values in tumors and organs and ratios are listed in Table 1. Due to the finding that high-contrast images of ALCAM-positive tumor-bearing mice can be obtained at 4 h post-injection of ^{64}Cu-DOTA-anti-ALCAM CysDb, all subsequent studies with the radiotracer, including those involving *Alcam*$^{-/-}$ mice, were performed at this earlier time point.

ROI analysis

Uptake values in positive tumors calculated from quantitative ROI analysis of 21 h images were determined to be 1.6 ± 0.2 %ID/g and 1.7 ± 0.4 %ID/g (HPAF-II and BxPC-3, respectively). These values were lower than the corresponding *ex vivo* biodistribution values ($p < 0.05$), but the disparity was consistent. ROI analysis uptake values and those

determined from the *ex vivo* biodistribution study are found in Table 2. ROI analysis of 4 h images revealed slightly lower uptake values ($p < 0.01$), with 1.5 ± 0.2 %ID/g for HPAF-II and 1.4 ± 0.5 %ID/g for BxPC-3, but ROI analysis of 4 and 21 h images showed that tumor-to-background ratios (4.6 ± 1.1 and 5.1 ± 1.7 for HPAF-II at 4 and 21 h, respectively; 5.4 ± 3.3 and 4.7 ± 3.2 for BxPC-3 at 4 and 21 h, respectively) were not significantly different at the two time points ($p > .5$ for both HPAF-II and BxPC-3).

Immunohistochemistry

Tumors were harvested from additional, untreated mice to confirm that the ALCAM status of each tumor type was consistent with that previously determined for each cell line. The immunohistochemistry (IHC) images in Figure 4b show that the HPAF-II and BxPC-3 tumors stain positive for ALCAM, while the C6 tumor does not, as expected.

Discussion

Anti-ALCAM CysDb was successfully engineered, expressed, produced, and purified. As there continues to be a trend in the clinical setting towards using fully human antibodies (as opposed to murine, chimeric, or humanized antibodies) [28], it is important to note that anti-ALCAM CysDb is a fully human CysDb. The ease with which the CysDb gene construct was engineered using the phage display-derived scFv shows the utility of display technology in the quick and straightforward production of larger antibody fragments. Anti-ALCAM CysDb further differs from existing CysDbs (targeting anti-carcinoembryonic antigen (CEA), human epidermal growth factor receptor 2 (HER2), or CD20) [5,6] in its V_H-to-V_L domain orientation, unique amino acid sequence between the second variable domain and C-terminal cysteine (GAAAG compared to GG), and hexahistidine tag. The opposite variable domain orientation and different C-terminal amino acid sequence demonstrate the flexibility of the CysDb format, and the availability of the His tag, along with the finding that it neither interferes with the formation of a covalent dimer nor negatively affects protein yield, suggests that addition of such a tag could help streamline CysDb production and characterization.

Biochemical characterization of anti-ALCAM CysDb confirmed production of a covalent dimer, and *in vitro* functional analysis demonstrated specific binding of anti-ALCAM CysDb to ALCAM-positive cell lines, with a relatively high apparent affinity in the range of 1–3 nM. Previous work has shown that low nanomolar affinity is suitable for diabody PET imaging [29], and a modeling analysis based on data in the literature indicates that affinity maturation is not expected to result in higher uptake by positive tumors [30]. Due to published data showing that ALCAM undergoes internalization, a residualizing radiolabeling approach was employed, using DOTA as the chelating agent for the positron-emitter copper-64. Despite achieving high labeling efficiency, specific activity of the radiotracer was low. Different labeling conditions are currently being investigated in an effort to improve the specific activity of ^{64}Cu-DOTA-anti-ALCAM CysDb. Small animal PET images acquired at 4 h post-injection showed specific targeting of ALCAM-positive tumors in mice, a finding confirmed by *ex vivo* biodistribution studies. Positive tumor uptake levels at 21 h were comparable to those recently observed with a variety diabody radiotracers, including an ^{18}F-labeled anti-CEA diabody [4], a ^{68}Ga-labeled anti-EpCAM diabody [31], and an ^{111}In-labeled anti-mindin/GR-1 diabody [32]. Importantly, there was a general correspondence between the uptake values determined from the *ex vivo* biodistribution and ROI analyses, with the inherent subjectivity in drawing ROIs likely responsible for the slight differences in these values. This agreement in values exemplifies the quantitative potential of PET, a feature that makes this imaging modality an attractive choice for clinical applications.

The accumulation of activity in the liver is a common occurrence for copper-64-labeled probes [33], and is likely partially due to transchelation of the radionuclide from DOTA to metal-binding proteins in the liver, such as superoxide dismutase (SOD) and metallothionein [33,34]. Uptake values in the liver are typically less than 4% ID/g by 12 post-injection, if not earlier, for radiometal-labeled diabodies [31,32,35], suggesting that an additional factor contributed to the higher hepatic levels seen in the present work. A recent comparative biodistribution analysis of two HER2-targeting Affibody variants, one containing and the other lacking an N-terminal hexahistidine tag, showed higher uptake values in the liver for the variant possessing a His tag [36]. We are currently investigating the possibility that the presence of the C-terminal His tag on anti-ALCAM CysDb is similarly leading to elevated liver levels. The strong kidney signals on the 4 h microPET images are expected due to the renal clearance of the 50 kDa protein [37], and the corresponding uptake levels at 21 h are typical of diabody probes [31,32,35]. *Ex vivo* biodistribution analysis at 4 h post-injection of ^{64}Cu-DOTA-anti-ALCAM CysDb in female *Alcam*$^{-/-}$ mice confirmed that accumulation of the probe in the liver and kidneys is not due to ALCAM expression, as tracer uptake values for these organs were comparable to those seen in the tumor-bearing nude mice. These findings show promise for ALCAM as an imaging biomarker and demonstrate that ^{64}Cu-DOTA-anti-ALCAM CysDb is a suitable agent for same-day PET imaging of xenografts that exhibit membranous ALCAM expression. Additionally, anti-ALCAM CysDb is cross-reactive with the murine antigen (data not shown), which would facilitate studies with mouse models of cancer that better recapitulate human disease. Looking forward, the direct translation of ^{64}Cu-DOTA-anti-ALCAM CysDb to the clinic would be unlikely due to several factors, including the limited production and relatively short half-life of copper-64, and the potential problem of nephrotoxicity due to high renal exposure to the beta-emitting radionuclide. Furthermore, the high hepatic activity levels seen in this study would preclude the use of ^{64}Cu-DOTA-anti-ALCAM CysDb in detecting liver metastases. As the rate of ALCAM internalization appears to be relatively slow [38], imaging with ^{18}F-labeled (non-residualizing) anti-ALCAM CysDb should be feasible and could be a solution to these limitations. The potential advantages of labeling with fluorine-18, the most widely used PET radionuclide in the clinic, have been demonstrated by the high-contrast imaging and low renal and hepatic activity levels (< 3% ID/g at 4 h post-injection) seen with ^{18}F-labeled anti-carcinoembryonic antigen (CEA) [4] and –prostate stem cell antigen (PSCA) [39] diabodies.

Pancreatic adenocarcinoma is the fourth leading cause of cancer-related deaths in the United States [40]. Earlier detection and the ability to stage disease accurately could improve the survival rate for patients with the malignancy, making it one that could benefit greatly from an imaging agent. Currently, the imaging modalities most frequently used in the assessment of pancreatic adenocarcinoma are computed tomography (CT), magnetic resonance imaging (MRI), and 2-[^{18}F] Fluoro-2-deoxy-D-glucose positron emission tomography (FDG-PET). While CT/MRI is effective in evaluating local disease, it is often inadequate for delineating biology or detecting metastatic spread [41]. FDG-PET is most useful for detecting metastatic disease and disease recurrence, but shortcomings include missing liver metastases and incorrectly diagnosing patients with chronic pancreatitis [41]. Imaging agents that are specific to cell surface proteins on tumors cells could provide the specificity needed for improved detection and staging of pancreatic adenocarcinoma, along with evidence of a true tumor target for therapy. Recently, promising results in the preclinical setting have been obtained with a variety of such imaging agents, including an intact antibody-based anti-prostate stem cell antigen (PSCA) single photon emission computed tomography (SPECT) probe [42], anti-$\alpha_v\beta_6$ peptide [43] and intact antibody-based anti-carcinoembryonic antigen-related cell adhesion molecule (CEACAM) 6 [44] PET probes, and intact antibody-based anti-$\alpha_v\beta_5$ [45]and anti-mucin 1 (MUC1) [46] gamma imaging agents. This work adds ALCAM to the list of successfully imaged pancreatic cancer biomarkers.

The functionality of a PET probe is dependent upon its ability to reach and bind its target, making the accessibility of an imaging biomarker a critical factor. Since antibody PET probes will only encounter cell surface molecules, candidate targets should exhibit some degree of cell membrane localization. An ideal imaging biomarker should also be expressed at an abnormally high level in the diseased state. Pancreatic adenocarcinoma was the malignancy chosen for evaluation of ALCAM as an imaging biomarker due to the high cell surface expression of ALCAM on HPAF-II and BxPC-3 cells as determined by quantitative flow cytometry, as well as the apparent clinical relevance demonstrated by a proteomic profiling study showing ALCAM to be differentially expressed 2.54-fold in pancreatic cancer tissue compared to normal pancreatic tissue [13]. It is important to note that in this profiling study, cellular localization of ALCAM was not specified. In a more recent report, Kahlert *et al* performed large-scale IHC analysis of ALCAM expression on clinical specimens [47]. The IHC study revealed that 58% (56/97) of the pancreatic cancer tissue samples and 80% (48/60) of the normal pancreatic tissue samples were ALCAM-positive, and a positive correlation was found between increased ALCAM expression on pancreatic cancer tissue and both poor survival and early relapse after surgical resection. While ALCAM expression on normal pancreatic tissue was determined to be mainly cell surface, expression on cancerous tissue was predominantly cytoplasmic, aside from a small number of patients whose tumors exhibited both membranous and cytoplasmic ALCAM expression. Given these more detailed findings, pancreatic adenocarcinoma may not be the disease that could benefit most from imaging with ^{64}Cu-DOTA-anti-ALCAM CysDb PET.

Due to the classification of ALCAM as a potential pan-cancer biomarker, much effort is currently being focused on determining the biological role of the protein as well as its potential as a diagnostic or prognostic marker. Additionally, success with targeted anti-ALCAM therapeutics, including an anti-ALCAM scFv liposomal drug conjuguate that exhibited a cytotoxic effect on prostate cancer cells *in vitro* [22] and, more recently, an anti-ALCAM scFv that inhibited tumor growth in an animal model of colorectal carcinoma [48], suggests that ALCAM could serve as a therapeutic target. As ALCAM expression and localization data is generated for malignancies, it will become clearer which could benefit from a targeted therapeutic and complementary molecular imaging agent. Of the diseases for which this information is presently available, colorectal carcinoma appears to be a promising candidate thus far for lesion detection using ^{64}Cu-DOTA-anti-ALCAM CysDb PET imaging. In an IHC study by Weichert *et al*, normal colon mucosa exhibited a low level of cytoplasmic ALCAM expression, while 59% and 31% of cancerous colorectal tissue showed upregulation of cytoplasmic and membranous ALCAM, respectively [10]. Importantly, the authors also found a positive correlation between membranous ALCAM expression and reduced survival. This pattern of expression makes ALCAM a promising *in vivo* imaging marker for colorectal cancer, and animal imaging studies with ^{64}Cu-DOTA-anti-ALCAM CysDb and mice bearing ALCAM-positive human colon carcinoma xenografts are underway.

Conclusions

^{64}Cu-DOTA-CysDb showed specific and rapid targeting and imaging of positive human pancreatic adenocarcinoma xenografts in mice, demonstrating that the CysDb format is conducive to same-day imaging applications and suggesting that further investigation of ALCAM as an imaging biomarker is warranted. Furthermore, the correspondence between the uptake values in positive tumors determined from the *ex vivo* biodistribution and ROI analyses exemplifies the quantitative potential of PET, a feature that makes this imaging modality an attractive choice for clinical applications.

Acknowledgments

Funding support was provided by the National Cancer Institute through the UCLA *in vivo* Cellular and Molecular Imaging Center (NIH CA 86306), the Stanford Center for Nanotechnology Excellence (NIH CA 119367), and the UCLA Small Animal Imaging Resource Program (NIH CA 92865), and a Dr. Ursula Mandel Scholarship. We thank Dr. Noah Federman for his help with the immunofluorescence experiments and Waldemar Ladno for his assistance with the animal studies. We would also like to acknowledge the UCLA Translational Pathology Core Laboratory for their antibody optimization and immunostaining services. Flow cytometry was performed in the UCLA Jonsson Comprehensive Cancer Center (JCCC) and Center for AIDS Research Flow Cytometry Core Facility, supported by NIH awards CA-16042 and AI-28697.

References

1. Wu AM. Antibodies and antimatter: the resurgence of immuno-PET. J Nucl Med. 2009; 50:2–5. [PubMed: 19091888]
2. Wu AM, Olafsen T. Antibodies for molecular imaging of cancer. Cancer J. 2008; 14:191–7. [PubMed: 18536559]
3. Wu AM, Senter PD. Arming antibodies: prospects and challenges for immunoconjugates. Nat Biotechnol. 2005; 23:1137–46. [PubMed: 16151407]
4. Cai W, Olafsen T, Zhang X, et al. PET imaging of colorectal cancer in xenograft-bearing mice by use of an 18F-labeled T84.66 anti-carcinoembryonic antigen diabody. J Nucl Med. 2007; 48:304–10. [PubMed: 17268029]
5. Olafsen T, Cheung CW, Yazaki PJ, et al. Covalent disulfide-linked anti-CEA diabody allows site-specific conjugation and radiolabeling for tumor targeting applications. Protein Eng Des Sel. 2004; 17:21–7. [PubMed: 14985534]
6. Sirk SJ, Olafsen T, Barat B, Bauer KB, Wu AM. Site-specific, thiol-mediated conjugation of fluorescent probes to cysteine-modified diabodies targeting CD20 or HER2. Bioconjug Chem. 2008; 19:2527–34. [PubMed: 19053310]
7. King JA, Ofori-Acquah SF, Stevens T, Al-Mehdi AB, Fodstad O, Jiang WG. Activated leukocyte cell adhesion molecule in breast cancer: prognostic indicator. Breast Cancer Res. 2004; 6:R478–87. [PubMed: 15318930]
8. Burkhardt M, Mayordomo E, Winzer KJ, et al. Cytoplasmic overexpression of ALCAM is prognostic of disease progression in breast cancer. J Clin Pathol. 2006; 59:403–9. [PubMed: 16484444]
9. Kulasingam V, Zheng Y, Soosaipillai A, Leon AE, Gion M, Diamandis EP. Activated leukocyte cell adhesion molecule: a novel biomarker for breast cancer. Int J Cancer. 2009; 125:9–14. [PubMed: 19322904]
10. Weichert W, Knosel T, Bellach J, Dietel M, Kristiansen G. ALCAM/CD166 is overexpressed in colorectal carcinoma and correlates with shortened patient survival. J Clin Pathol. 2004; 57:1160–4. [PubMed: 15509676]
11. Sawhney M, Matta A, Macha MA, et al. Cytoplasmic accumulation of activated leukocyte cell adhesion molecule is a predictor of disease progression and reduced survival in oral cancer patients. Int J Cancer. 2009; 124:2098–105. [PubMed: 19142865]
12. Mezzanzanica D, Fabbi M, Bagnoli M, et al. Subcellular localization of activated leukocyte cell adhesion molecule is a molecular predictor of survival in ovarian carcinoma patients. Clin Cancer Res. 2008; 14:1726–33. [PubMed: 18347173]
13. Chen R, Yi EC, Donohoe S, et al. Pancreatic cancer proteome: the proteins that underlie invasion, metastasis, and immunologic escape. Gastroenterology. 2005; 129:1187–97. [PubMed: 16230073]
14. Kristiansen G, Pilarsky C, Wissmann C, et al. ALCAM/CD166 is up-regulated in low-grade prostate cancer and progressively lost in high-grade lesions. Prostate. 2003; 54:34–43. [PubMed: 12481253]
15. Kristiansen G, Pilarsky C, Wissmann C, et al. Expression profiling of microdissected matched prostate cancer samples reveals CD166/MEMD and CD24 as new prognostic markers for patient survival. J Pathol. 2005; 205:359–76. [PubMed: 15532095]

16. Patel DD, Wee SF, Whichard LP, et al. Identification and characterization of a 100-kD ligand for CD6 on human thymic epithelial cells. J Exp Med. 1995; 181:1563–8. [PubMed: 7535342]
17. Bowen MA, Patel DD, Li X, et al. Cloning, mapping, and characterization of activated leukocyte-cell adhesion molecule (ALCAM), a CD6 ligand. J Exp Med. 1995; 181:2213–20. [PubMed: 7760007]
18. van Kempen LC, Meier F, Egeblad M, et al. Truncation of activated leukocyte cell adhesion molecule: a gateway to melanoma metastasis. J Invest Dermatol. 2004; 122:1293–301. [PubMed: 15140234]
19. van Kilsdonk JW, Wilting RH, Bergers M, et al. Attenuation of melanoma invasion by a secreted variant of activated leukocyte cell adhesion molecule. Cancer Res. 2008; 68:3671–9. [PubMed: 18483249]
20. Liu B, Conrad F, Cooperberg MR, Kirpotin DB, Marks JD. Mapping tumor epitope space by direct selection of single-chain Fv antibody libraries on prostate cancer cells. Cancer Res. 2004; 64:704–10. [PubMed: 14744788]
21. Liu B, Conrad F, Roth A, Drummond DC, Simko JP, Marks JD. Recombinant full-length human IgG1s targeting hormone-refractory prostate cancer. J Mol Med. 2007; 85:1113–23. [PubMed: 17554518]
22. Roth A, Drummond DC, Conrad F, et al. Anti-CD166 single chain antibody-mediated intracellular delivery of liposomal drugs to prostate cancer cells. Mol Cancer Ther. 2007; 6:2737–46. [PubMed: 17938267]
23. Galfre G, Milstein C. Preparation of monoclonal antibodies: strategies and procedures. Methods Enzymol. 1981; 73:3–46. [PubMed: 7300683]
24. Olafsen T, Gu Z, Sherman MA, et al. Targeting, imaging, and therapy using a humanized antiprostate stem cell antigen (PSCA) antibody. J Immunother. 2007; 30:396–405. [PubMed: 17457214]
25. Bebbington CR, Renner G, Thomson S, King D, Abrams D, Yarranton GT. High-level expression of a recombinant antibody from myeloma cells using a glutamine synthetase gene as an amplifiable selectable marker. Biotechnology (N Y). 1992; 10:169–75. [PubMed: 1369477]
26. Olafsen T, Kenanova VE, Sundaresan G, et al. Optimizing radiolabeled engineered anti-p185HER2 antibody fragments for in vivo imaging. Cancer Res. 2005; 65:5907–16. [PubMed: 15994969]
27. Loening AM, Gambhir SS. AMIDE: a free software tool for multimodality medical image analysis. Mol Imaging. 2003; 2:131–7. [PubMed: 14649056]
28. Nelson AL, Dhimolea E, Reichert JM. Development trends for human monoclonal antibody therapeutics. Nat Rev Drug Discov. 2010; 9:767–74. [PubMed: 20811384]
29. Leyton JV, Olafsen T, Sherman MA, et al. Engineered humanized diabodies for microPET imaging of prostate stem cell antigen-expressing tumors. Protein Eng Des Sel. 2009; 22:209–16. [PubMed: 18957406]
30. Schmidt MM, Wittrup KD. A modeling analysis of the effects of molecular size and binding affinity on tumor targeting. Mol Cancer Ther. 2009; 8:2861–71. [PubMed: 19825804]
31. Eder M, Knackmuss S, Le Gall F, et al. (68)Ga-labelled recombinant antibody variants for immuno-PET imaging of solid tumours. Eur J Nucl Med Mol Imaging. 2010
32. Schneider DW, Heitner T, Alicke B, et al. In vivo biodistribution, PET imaging, and tumor accumulation of 86Y- and 111In-antimindin/RG-1, engineered antibody fragments in LNCaP tumor-bearing nude mice. J Nucl Med. 2009; 50:435–43. [PubMed: 19223400]
33. Anderson CJ, Ferdani R. Copper-64 radiopharmaceuticals for PET imaging of cancer: advances in preclinical and clinical research. Cancer Biother Radiopharm. 2009; 24:379–93. [PubMed: 19694573]
34. Shokeen M, Anderson CJ. Molecular imaging of cancer with copper-64 radiopharmaceuticals and positron emission tomography (PET). Acc Chem Res. 2009; 42:832–41. [PubMed: 19530674]
35. Yazaki PJ, Wu AM, Tsai SW, et al. Tumor targeting of radiometal labeled anti-CEA recombinant T84.66 diabody and t84.66 minibody: comparison to radioiodinated fragments. Bioconjug Chem. 2001; 12:220–8. [PubMed: 11312683]

36. Ahlgren S, Wallberg H, Tran TA, et al. Targeting of HER2-expressing tumors with a site-specifically 99mTc-labeled recombinant affibody molecule, ZHER2:2395, with C-terminally engineered cysteine. J Nucl Med. 2009; 50:781–9. [PubMed: 19372467]
37. Arano Y. Strategies to reduce renal radioactivity levels of antibody fragments. Q J Nucl Med. 1998; 42:262–70. [PubMed: 9973841]
38. Piazza T, Cha E, Bongarzone I, et al. Internalization and recycling of ALCAM/CD166 detected by a fully human single-chain recombinant antibody. J Cell Sci. 2005; 118:1515–25. [PubMed: 15769845]
39. Liu K, Lepin EJ, Wang M-W, Guo F, Lin W-Y, Chen Y-C, Sirk SJ, Olma S, Phelps ME, Zhao X-Z, Tseng H-R, van Dam RM, Wu AM, Shen CK-F. Microfluidic-Based ^{18}F Labeling of Biomolecules for Immuno-Positron Emission Tomography. Molecular Imaging. 10:2011.10.2310/7290.2010.00043
40. Horner, MJRL.; Krapcho, M.; Neyman, N.; Aminou, R.; Howlader, N.; Altekruse, SF.; Feuer, EJ.; Huang, L.; Mariotto, A.; Miller, BA.; Lewis, DR.; Eisner, MP.; Stinchcomb, DG.; Edwards, BK. SEER Cancer Statistics Review, 1975–2006. National Cancer Institute; Bethesda, MD: http://seer.cancer.gov/csr/1975_2006/, based on November 2008 SEER data submission, posted to the SEER web site, 2009
41. Parsons CM, Sutcliffe JL, Bold RJ. Preoperative evaluation of pancreatic adenocarcinoma. J Hepatobiliary Pancreat Surg. 2008; 15:429–35. [PubMed: 18670846]
42. Foss CA, Fox JJ, Feldmann G, et al. Radiolabeled anti-claudin 4 and anti-prostate stem cell antigen: initial imaging in experimental models of pancreatic cancer. Mol Imaging. 2007; 6:131–9. [PubMed: 17445507]
43. Hausner SH, Abbey CK, Bold RJ, et al. Targeted in vivo imaging of integrin alphavbeta6 with an improved radiotracer and its relevance in a pancreatic tumor model. Cancer Res. 2009; 69:5843–50. [PubMed: 19549907]
44. Strickland LA, Ross J, Williams S, et al. Preclinical evaluation of carcinoembryonic cell adhesion molecule (CEACAM) 6 as potential therapy target for pancreatic adenocarcinoma. J Pathol. 2009; 218:380–90. [PubMed: 19334050]
45. Vervoort L, Burvenich I, Staelens S, et al. Preclinical evaluation of monoclonal antibody 14C5 for targeting pancreatic cancer. Cancer Biother Radiopharm. 2010; 25:193–205. [PubMed: 20423233]
46. Mariani G, Molea N, Bacciardi D, et al. Initial tumor targeting, biodistribution, and pharmacokinetic evaluation of the monoclonal antibody PAM4 in patients with pancreatic cancer. Cancer Res. 1995; 55:5911s–5915s. [PubMed: 7493369]
47. Kahlert C, Weber H, Mogler C, et al. Increased expression of ALCAM/CD166 in pancreatic cancer is an independent prognostic marker for poor survival and early tumour relapse. Br J Cancer. 2009; 101:457–64. [PubMed: 19603023]
48. Wiiger MT, Gehrken HB, Fodstad O, Maelandsmo GM, Andersson Y. A novel human recombinant single-chain antibody targeting CD166/ALCAM inhibits cancer cell invasion in vitro and in vivo tumour growth. Cancer Immunol Immunother. 2010

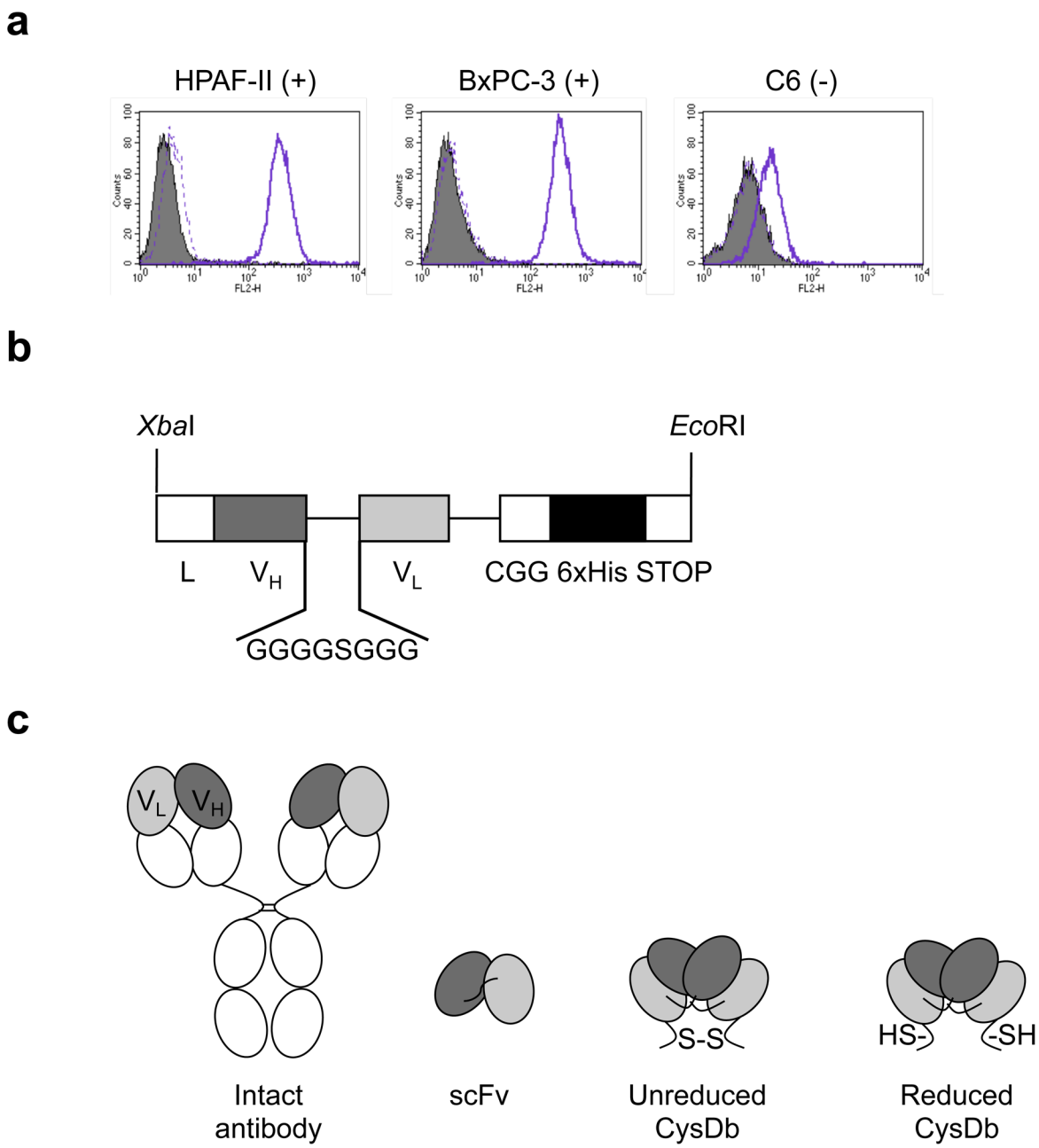

Figure 1.

a, Determination of ALCAM expression by flow cytometry. *Left*, HPAF-II; *middle*, BxPC-3; *right*, C6. *Filled peak*, cells only. *Solid line*, cells incubated with mouse anti-human CD166 monoclonal antibody, followed by FITC-conjugated goat anti-mouse antibody. *Dashed line*, cells incubated with only FITC-conjugated goat anti-mouse antibody. *b,* Anti-ALCAM CysDb gene construct showing restriction sites for pEE12 cloning, mammalian leader sequence for protein secretion, 8-aa linker, C-terminal cysteine, and hexahistidine tag. *c*, Schematic representations of (from left to right) an intact antibody, scFv, unreduced CysDb, and reduced CysDb.

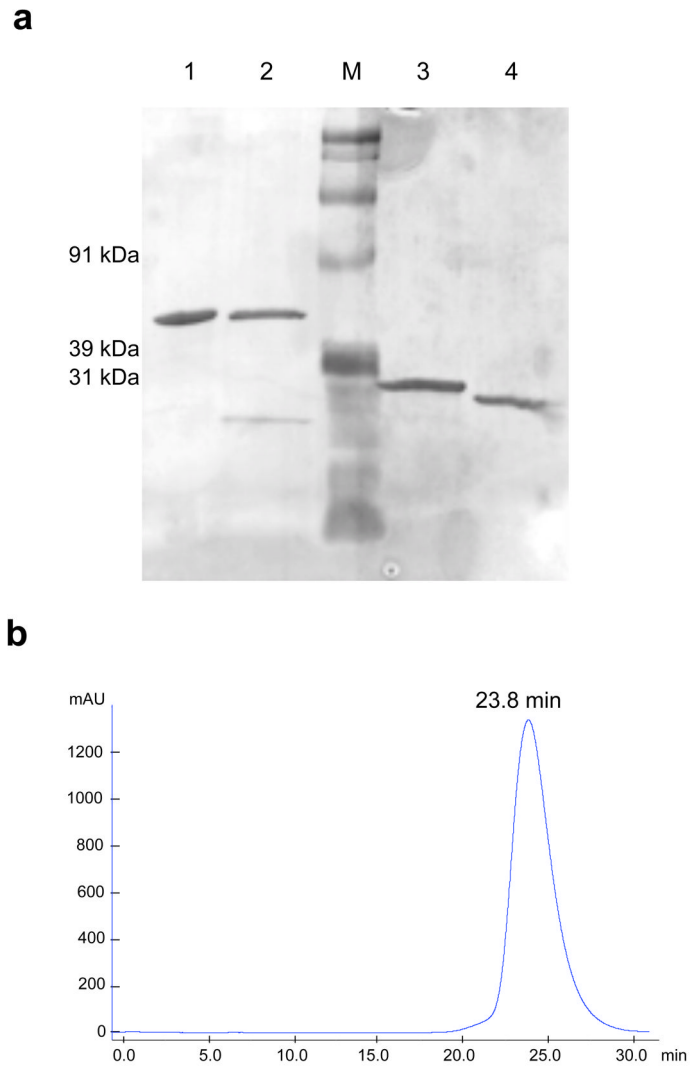

Figure 2.

Biochemical characterization of anti-ALCAM CysDb. *a*, SDS-PAGE analysis of anti-ALCAM CysDb and, for comparison, anti-HER2 CysDb (*1*, anti-HER2 CysDb; *2*, anti-ALCAM CysDb; *M*, marker; *3*, reduced anti-HER2 CysDb; *4*, reduced anti-ALCAM CysDb). *b*, Size exclusion chromatography elution profile of anti-ALCAM CysDb on Superdex 75.

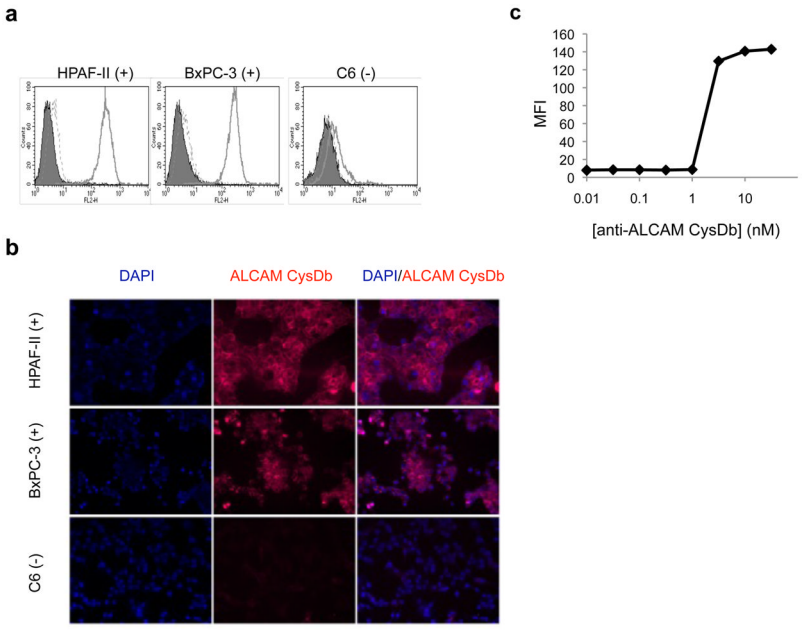

Figure 3.

Functional characterization of anti-ALCAM CysDb. *a*, Evaluation of binding specificity by flow cytometry. *Left*, HPAF-II; *middle*, BxPC-3; *right*, C6. *Filled peak*, cells only. *Solid line*, cells incubated with anti-ALCAM CysDb, followed by mouse anti-Penta-His antibody and PE-conjugated goat anti-mouse antibody. *Dashed line*, cells incubated with only mouse anti-Penta-His antibody and PE-conjugated goat anti-mouse antibody. *b*, Evaluation of binding to cultured cells by immunofluorescence. *Top panels*, HPAF-II; *middle panels*, BxPC-3; *bottom panels*, C6. *Left column*, DAPI staining. *Middle column*, Alexa Fluor 647-anti-ALCAM CysDb staining. *Right column*, overlay. *c*, Determination of K_D by flow cytometry.

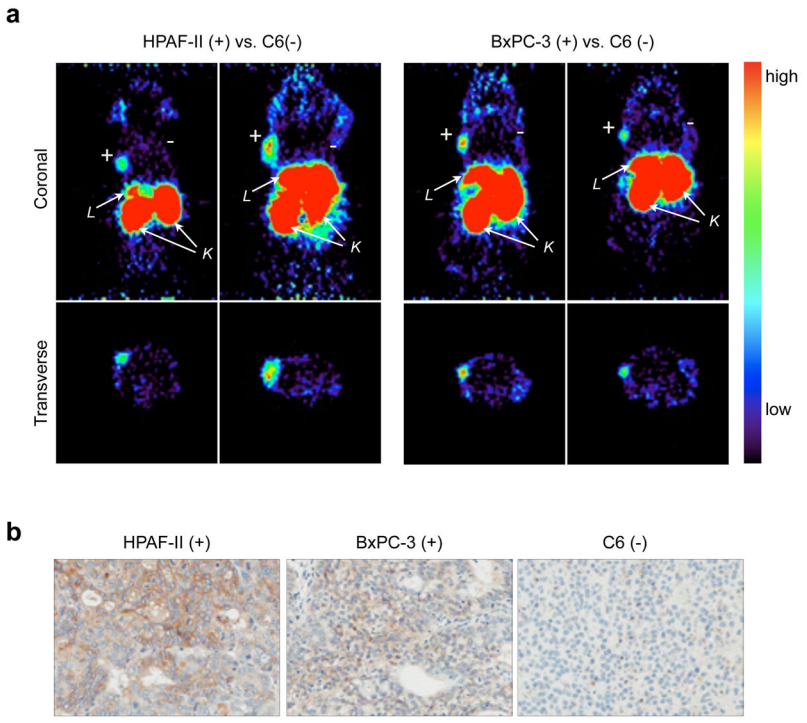

Figure 4.

a, MicroPET images of female nude mice bearing HPAF-II (*left two panels*) or BxPC-3 (*right two panels*) subcutaneous xenografts in the left shoulder region, and C6 subcutaneous xenografts in the right shoulder region at 4 h post-injection of ^{64}Cu-DOTA-anti-ALCAM CysDb. Upper and lower panels are coronal and transverse slices, respectively. *L*, liver; *K*, kidney. *b*, *Ex vivo* immunohistochemistry of tumors. Sections of xenografts stained for ALCAM (*left*, HPAF-II; *middle*, BxPC-3; *right*, C6).

Table 1

Biodistribution of ^{64}Cu-DOTA-anti-ALCAM CysDb at 21 h in female nude mice bearing ALCAM-positive (HPAF-II or BxPC-3) and ALCAM-negative (C6) tumors and at 4 h in non-tumor-bearing female *Alcam*$^{-/-}$ mice.

	% ID/g (mean ± SD)		
	HPAF-II (*n* = 5)	**BxPC-3 (*n* = 4)**	***Alcam*$^{-/-}$ (*n* = 2)**
Tissue	**21 h**	**21 h**	**4 h**
Positive tumor (T)	1.8 ± 0.5	2.5 ± 0.5	
Negative tumor (C6)	1.0 ± 0.1	1.0 ± 0.1	
Liver	6.6 ± 0.5	6.8 ± 1.4	5.4 ± 0.1
Spleen	1.7 ± 0.2	1.8 ± 0.3	2.2 ± 0.7
Kidneys	42 ± 5.0	40 ± 0.8	90 ± 3.5
Lung	1.8 ± 0.5	2.3 ± 0.3	2.1 ± 0.3
Blood	0.7 ± 0.1	0.9 ± 0.1	1.0 ± 0.3
Carcass	0.8 ± <0.1	1.0 ± 0.1	1.4 ± 0.2
Ratios			
T/blood	2.5 ± 0.9	2.9 ± 0.6	
T/C6	1.9 ± 0.6	2.4 ± 0.6	

Table 2

Comparison of uptake values in positive tumors determined by region of interest (ROI) and *ex vivo* biodistribution (BD) analyses.

Tumor	% ID/g		
	ROI (4 h)	**ROI (21 h)**	***Ex vivo* BD (21 h)**
HPAF-II			
Mouse 1	1.3	1.4	1.2
Mouse 2	1.5	1.6	2.3
Mouse 3	1.7	1.8	2.3
Mean % ID/g ± SD	*1.5 ± 0.2*	*1.6 ± 0.2*	*1.8 ± 0.5*
BxPC-3			
Mouse 1	1.3	1.7	1.8
Mouse 2	1.9	2.0	3.1
Mouse 3	1.6	1.9	2.6
Mouse 4	0.9	1.2	2.5
Mean % ID/g ± SD	*1.4 ± 0.5*	*1.7 ± 0.4*	*2.5 ± 0.5*